UNIVERSITY OF OKLAHOMA

GRADUATE COLLEGE

HOMER L. DODGE DEPARTMENT OF PHYSICS AND ASTRONOMY

Searching for Supersymmetric Particles at the Large Hadron Collider using the ATLAS Detector

A DISSERTATION

SUBMITTED TO THE GRADUATE FACULTY

in partial fulfillment of the requirements for the

Degree of

DOCTOR OF PHILOSOPHY

By

OTHMANE RIFKI
Norman, Oklahoma
2016

Table of Contents

List of Tables

List of Figures

1 Overview

As part of our quest to understand and describe the physical world we live in, human beings embarqued on a journey to search for the most fundamental constituents of matter, describe their interactions, and predict their behavior. In short, we want to answer the question "what is matter made of?" The last few decades represented a revolutionary period in the study of fundamental physics. Several particle accelerators became operational and allowed us to disentangle the structure of matter down to a handful of constituents we call elementary particles. The most powerful of these accelerators is is the Large Hadron Collider (LHC) at CERN . The basic idea of the LHC and other accelerators is to collide particles, in our case protons, at very high energies and take snapshots of these collisions. The goal is to guess the form of the interactions happening in each collision and compare the resulting theoretical predictions with the results of our snapshots of the collision, called the experimental data. This is one of the strategies that led us to formulate a mathematical framework that describes the elementary particles and their interactions which is known as the Standard Model of elementary particles (SM). When subjected to experimental tests, the SM successfully describes three of the four fundamental forces: electromagnetic, weak, and strong interactions. On the other hand, the SM is not believed to be complete since it fails to explain a number of problems that are still facing today's physics community. First, the SM does not incorporate the fourth fundamental force of gravity. Moreover, It does not provide insight on the nature of the "invisible"

matter that is holding galaxies together, which constitutes $\sim 26\%$ of the energy density of the universe and is known as *Dark Matter*. In addition, the SM does not account for the different masses and mixing of the 12 leptons known as the *flavor problem*, and the predominance of matter over antimatter. In order to solve these problems, searches for physics not accounted for by the SM have been pursued at the LHC. The aim is to conduct searches for new states of matter from the experimental data and compare it to theoretical models that predict the existence of these new states of matter. The experimental data used in our analysis has been collected by the ATLAS detector which is one of the most complex particle detectors ever designed. ATLAS takes snapshots of the collisions that are happening 40 million times per second and reconstruct what happened in the collision. We analyze this information to test if the theoretical models that we are considering are compatible with our experimental data. One of the theories that predict the existence of new states of matter is supersymmetry. Supersymmetry is based on a fundamental symmetry between the elementary particles and the particles that mediate their interactions.

In the remainder of this document, I present an anlysis of data collected by the ATLAS experiment with the aim of comparing it with theoretical predictions based on supersymmetric theories. The level of detail is intended for the professional scientific audience.

2 Introduction

Supersymmetry (SUSY) is a theoretically favoured extension of the Standard Model (SM), which for each degree of freedom of the SM predicts another degree of freedom with a different spin. These degrees of freedom combine into physical superpartners of the SM particles: scalar partners of quarks and leptons (squarks ($\tilde{q}$) and sleptons), fermionic partners of gauge and Higgs bosons (gluinos ($\tilde{g}$), charginos ($\tilde{\chi}_i^{\pm}$, with $i = 1,2$) and neutralinos ($\tilde{\chi}_i^0$ with $i = 1,2,3,4$)), all with identical quantum numbers to their SM partners, except spin. Since no superpartner of any of the SM particles has been observed yet, SUSY must be a broken symmetry at some higher energy scale.

The discovery (or exclusion) of weak-scale SUSY is one of the highest physics priorities for the LHC. The primary target for early supersymmetry searches in proton-proton (pp) collisions at a centre-of-mass energy of 13 TeV at the LHC, given their large expected cross-section, is the strong production of gluinos and squarks. In order for supersymmetry to provide a solution to the hierarchy problem of the SM, the supersymmetric partners of the top and bottom quarks are expected to be light and within reach of the LHC.

Under the hypothesis of R-parity conservation , SUSY partners are produced in pairs and decay to the Lightest Supersymmetric Particle (LSP) which is stable and, in large variety of models, is assumed to be the lightest neutralino ($\tilde{\chi}_1^0$) which escapes detection. The undetected $\tilde{\chi}_1^0$ would result in substantial missing transverse momentum ($E_{\mathrm{T}}^{\mathrm{miss}}$), while the rest of the cascade, originating from the

decays of squarks and gluinos, would yield final states with multiple jets and possibly leptons.

In this analysis, events containing multiple jets and either two leptons (electrons or muons) of the same electric charge (same-sign leptons, SS) or at least three leptons (3L) are used to search for strongly produced supersymmetric particles. Signatures with SS or 3L are predicted in many SUSY scenarios. Gluinos produced in pairs or in association with a squark can lead to SS signatures when decaying to any final state that includes leptons because gluinos are Majorana fermions. Squark production, directly in pairs or through $\tilde{g}\ \tilde{g}$ or $\tilde{g}\ \tilde{q}$ production with subsequent $\tilde{g} \rightarrow q\tilde{q}$ decay, can also lead to SS or 3L signatures when the squarks decay in cascades involving top quarks (t), charginos, neutralinos or sleptons, which subsequently decay as $t \rightarrow bW$, $\tilde{\chi}_i^{\pm} \rightarrow W^{\pm(*)}\tilde{\chi}_j^0$, $\tilde{\chi}_i^0 \rightarrow h/Z^{(*)}\tilde{\chi}_j^0$, or $\tilde{\ell} \rightarrow \ell\tilde{\chi}_1^0$, respectively. Since this search benefits from low SM backgrounds, it allows the use of relatively loose kinematic requirements on $E_{\mathrm{T}}^{\mathrm{miss}}$, increasing the sensitivity to scenarios with small mass differences between SUSY particles (compressed scenarios) or where R-parity is violated. This search is thus sensitive to a wide variety of models based on very different assumptions.

This note presents the analysis of the 2015 dataset. Previous Run-2 preparation studies performed with DC14 samples can be found in . The Run-1 search for strongly produced SUSY particles with SS/3L was conducted using data from the full 2012 data-taking period (20.3 fb^{-1} at $\sqrt{s}$=8 TeV) . In that result, exclusion limits were placed on 15 different models. Gluino-mediated top squark scenarios, favoured by naturalness arguments, were excluded for $m_{\tilde{g}} <$ [600–1000] GeV ,

largely independently of the top squark mass and decay mode. Similar limits were placed on gluino-mediated production of first- and second-generation quarks for $m_{\tilde{\chi}_1^0} <$ [300–600] GeV . Limits were also placed on pair-production of bottom squarks and squarks of the first and second generations decaying in long cascades. In this new set of results using 2015 data, no significant excess is observed, and we extend the Run-1 exclusion limits for several SUSY models.

. In that result, exclusion limits were placed on 15 different models.

3 Signal models

3.1 Signal models considered in this analysis

Final states with two same-sign leptons and multiple jets are sensitive to a variety of new physics scenarios. In supersymmetric models in particular, such final states can be produced in the decays of heavy superpartners involving massive gauge bosons, sleptons or top quarks. We list in this section the different simplified models which we used as benchmarks to define our signal regions.

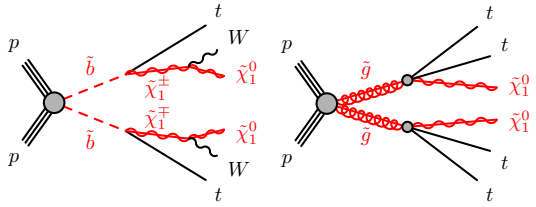

Figure 1: SUSY signal benchmarks leading to multiple b-jets : direct sbottom pair production decaying to top + chargino (left), and gluino decay via offshell stop (right).

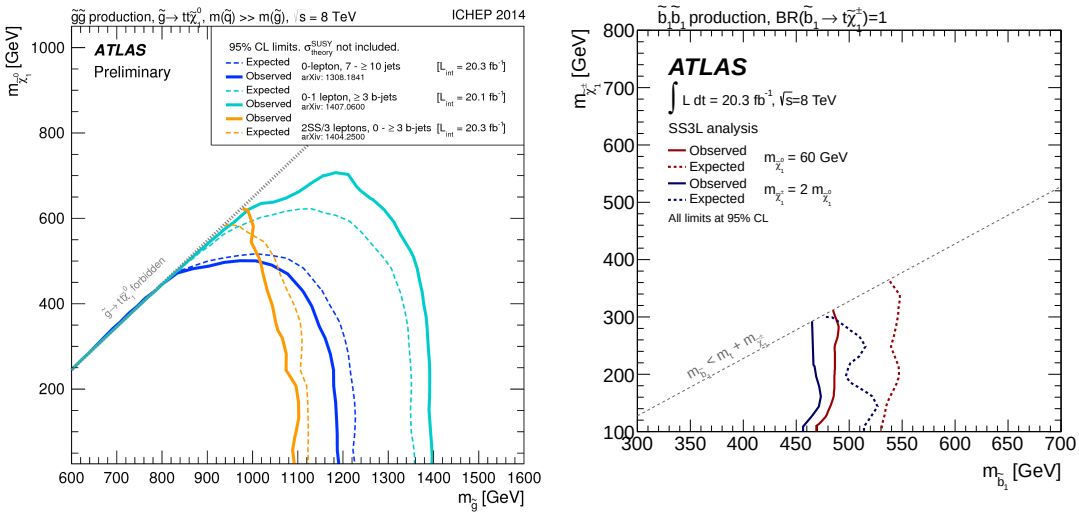

Figure 2: Exclusion limits on the gluino-stop offshell (left) and direct sbottom (right) scenarios set by ATLAS with the 2012 dataset .

Direct sbottom $\tilde{b}_1 \to t\tilde{\chi}_1^{\pm}$

In this model, bottom squarks are rather light and assumed to decay in a top quark and a chargino $\tilde{\chi}_1^{\pm}$ (Fig. 1), providing complementarity to the mainstream search which focuses on the channel $\tilde{b}_1 \to b\tilde{\chi}_1^0$. The final state resulting from the production of a sbottom pair contains pairs of top quarks, of W bosons and of neutralinos. While this final state may lead to various experimental signatures, the model was considered in Run-1 only by the same-sign leptons and jets search, leading to the exclusion limits presented in Fig. 2. The signal grid generated with the MC15 configurations adopts different hypotheses on the SUSY mass spectrum than what was retained for Run-1: in the latter case two grids were proposed with either a fixed neutralino mass (60 GeV) or a fixed chargino-to neutralino mass ratio (2:1). The MC15 grid fixes the chargino-neutralino mass difference to 100 GeV, always allowing on-shell W bosons in the $\tilde{\chi}_1^{\pm} \to W\tilde{\chi}_1^0$ decay. The reduced

chargino-neutralino mass gap compared to the MC12 grids allows to study signal scenarios with heavy neutralinos, which were not considered previously. Only pair production of the lightest sbottom is considered, followed by an exclusive decay in the aforementioned channel.

Gluino-stop offshell $\tilde{g} \rightarrow t\bar{t}\tilde{\chi}_1^0$

In this model inspired by naturalness arguments, gluinos are coupling preferentially to stops which are lighter than the other squarks. Gluinos are however considered lighter than stops, and decay directly into a $t\bar{t}\tilde{\chi}_1^0$ triplet via a virtual stop (Fig. 1). The pair production of gluinos leads to a final state containing four top quarks and two neutralinos. This characteristic final state is accessible through various experimental signatures, which is why this model is commonly used as a benchmark to compare analyses sensitivities. The searches performed with Run-1 data , summarized in Fig. 2, showed that the same-sign leptons final state is competitive only at large neutralino mass. This region of the phase space is consequently given a particular attention in the choice of signal regions described further on. In the signal samples referenced in this document, the mass of the lightest stop is fixed to 10 TeV and is mostly a $\widetilde{t}_R$ state. Only gluino pair production is considered, followed by an exclusive decay in the aforementioned channel.

;

Gluinos decays via gauginos

Figure 3: SUSY signal benchmarks leading to no or few b-jets : gluino pair production followed by two-step decays via heavy gauge bosons or sleptons.

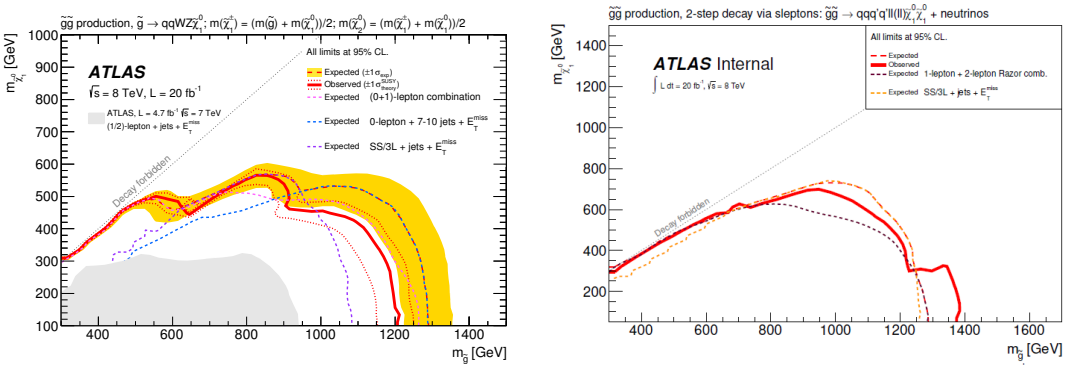

Figure 4: Exclusion limits on scenarios featuring gluino pair production followed by two-step decays via heavy gauge bosons or sleptons, set by ATLAS with the 2012 dataset .

These scenarios feature a less oriented search for gluinos, in the cases when they decay through gauginos in two steps, either via W and Z bosons ($\tilde{g} \rightarrow q\bar{q}'\tilde{\chi}_1^{\pm} \rightarrow q\bar{q}'W\tilde{\chi}_2^0 \rightarrow q\bar{q}'WZ\tilde{\chi}_1^0$) or sleptons ($\tilde{g} \rightarrow q\bar{q}'\tilde{\chi}_2^0 \rightarrow q\bar{q}\ell\tilde{\ell}/\nu\tilde{\nu} \rightarrow q\bar{q}'\ell\ell/\nu\nu\tilde{\chi}_1^0$). The b-jet multiplicity in these scenarios is low and they are used as benchmarks to define signal regions with b-jet vetoes.

In the first scenario, the final state is made of two W and two Z bosons (including offshell contributions), four additional jets and invisible particles (neutrinos and neutralinos). This generally leads to events with large jet multiplicities and a fair branching ratio for dileptonic final states. The exclusion limits obtained in

run-1 indeed illustrate the competitiveness of the SS/3L+jets search (Fig. 4 left). The signal grid is built with variable gluino and LSP masses, and the chargino and neutralino 2 masses are set such that the former lies half-way between the gluino and LSP masses, and the latter half-way between the chargino and LSP masses.

In the second scenario, the final state is made of charged leptons, four additional jets and invisible particles (neutrinos and neutralinos). The average jet multiplicity per event is smaller than in the previous scenario; another characteristic is the large fraction of events with several leptons, unlike most of the other scenarios that have a rather low acceptance due to the branching ratios of $W \to \ell\nu$ or $Z \to \ell\ell$. The exclusion limits obtained in run-1 (Fig. 4 right) show again that the SS/3L+jets final state is very competitive to probe those models. The signal grid is built with variable gluino and LSP masses; the $\tilde{\chi}_2^0$ mass is chosen half-way between the gluino and LSP masses, and the sleptons masses are also set equal and half-way between the $\tilde{\chi}_2^0$ and LSP masses. The $\tilde{\chi}_2^0$ may decay to any of the six sleptons ($\tilde{\ell}$, $\tilde{\nu}$) with equal probability. Noticeable changes have been introduced with respect to the run-1 grid. First, bottom squarks are no longer decoupled but are assumed to be mass-degenerate with the light-flavor squarks, opening the decay mode $\tilde{g} \to b\bar{b}\tilde{\chi}_2^0$ with 20% branching ratio. However, to simplify the model description we do not consider these decay modes; this translates concretely into vetoing events with $\tilde{g} \to b\bar{b}\tilde{\chi}_2^0$ decays and weighting the remaining events by a factor $1/(2 * 0.2 * 0.8 + 0.2^2)$ to readjust the branching ratios. Another more important change is that only gluino decays through $\tilde{\chi}_2^0$ are now considered in

Gluino mass (GeV)	500	550	600	650	700
Cross section (pb)	$27.4 \pm 14\%$	$15.6 \pm 14\%$	$9.20 \pm 14\%$	$5.60 \pm 14\%$	$3.53 \pm 14\%$
750	800	850	900	950	1000
$2.27 \pm 14\%$	$1.49 \pm 15\%$	$0.996 \pm 15\%$	$0.677 \pm 16\%$	$0.466 \pm 16\%$	$0.325 \pm 17\%$
1050	1100	1150	1200	1250	1300
$0.229 \pm 17\%$	$0.163 \pm 18\%$	$0.118 \pm 18\%$	$0.0856 \pm 18\%$	$0.0627 \pm 19\%$	$0.0461 \pm 20\%$
1350	1400	1450	1500	1550	1600
$0.0340 \pm 20\%$	$0.0253 \pm 21\%$	$0.0189 \pm 22\%$	$0.0142 \pm 23\%$	$0.0107 \pm 23\%$	$0.00810 \pm 24\%$

Sbottom mass (GeV)	400	450	500	550
Cross section (pb)	$1.84 \pm 14\%$	$0.948 \pm 13\%$	$0.518 \pm 13\%$	$0.296 \pm 13\%$
600	650	700	750	800
$0.175 \pm 13\%$	$0.107 \pm 13\%$	$0.0670 \pm 13\%$	$0.0431 \pm 14\%$	$0.0283 \pm 14\%$

Table 1: Signal cross-sections and related uncertainties for scenarios featuring gluino (top table) or sbottom (bottom table) pair production, as a function of the pair-produced superpartner mass, computed in .

the model generation, while in the run-1 model decays via charginos $\tilde{g} \rightarrow q\bar{q}'\tilde{\chi}_1^{\pm}$ (followed by $\tilde{\chi}_1^{\pm} \rightarrow \tilde{\ell}\nu/\ell\tilde{\nu}$) were also considered with a 50% branching ratio. The consequences of the latter change are quite important for this analysis, reducing the acceptance of inclusive trilepton selections by $\sim 30\%$.

Since both scenarios include non-resonant $W^* \rightarrow \ell\nu$ and $Z^* \rightarrow \ell\ell$ contributions, they also provide motivated benchmarks to gauge the analysis sensitivity for softer leptons p_T spectra, unlike the $\tilde{g} \rightarrow t\bar{t}\tilde{\chi}_1^0$ and $\tilde{b}_1 \rightarrow t\tilde{\chi}_1^{\pm}$ scenarios in which leptons always originate from on-shell W bosons hence can't be arbitrarily soft.

Models not considered for the moment

In the publications of the analysis results obtained with Run-1 data, exclusion limits were also provided for other signal models. These scenarios included notably simplified models such as $\tilde{g} \rightarrow tbW\tilde{\chi}_1^0$, $\tilde{g} \rightarrow tcW\tilde{\chi}_1^0$, squark pair production with similar decay modes as in the previous paragraph, as well as minimal models featuring R-parity violation through bilinear terms, gauge-mediated SUSY

breaking, or universal extra dimensions. These models are not considered for the moment, although interpretations might be proposed for them again in the future.

4 Signal region definition

The definitions of the signal regions have been studied to provide an optimal performance for $\sqrt{s} = 13$ TeV collisions and a low integrated luminosity (2-4 fb^{-1}). This optimization process was first performed with DC14 MC samples, and was then refined with the more accurate MC15 samples and close-to-final object definitions. We chose to categorize the signal regions based on their b-jet multiplicity, in continuation of the approach sustained in the Run-1 analysis:

- Signal region(s) with at least one b-jet ("SR1b"): these selections target signal scenarios involving top or bottom quarks, mostly related to third-generation squarks, such as the benchmark process $\tilde{b}_1\tilde{b}_1^* \to t\bar{t}\tilde{\chi}_1^+\tilde{\chi}_1^-$.

- Signal region(s) with at least three b-jets ("SR3b"): these selections target signal scenarios involving many top or bottom quarks, such as the benchmark process $\tilde{g}\ \tilde{g}\ \to t\bar{t}t\bar{t}\tilde{\chi}_1^0\tilde{\chi}_1^0$, and with their intrinsically very low background are particularly well suited for scenarios with compressed mass spectra.

- Signal region(s) with a b-jet veto ("SR0b"): these selections allow to increase the sensitivity to signal scenarios without bottom quarks, by suppressing most of the top background – the selections are then dominated by diboson background.

One can notice that there is no dedicated selection for final states with ≥ 2 b-jets: it is found to not be particularly useful, as the background is generally dominated by $t\bar{t} + X$ processes, which does not change substantially between ≥ 1 and ≥ 2 b-jets selections. By contrast the difference between ≥ 1 and ≥ 3 b-jets selections is very important.

To this first classification we add minimal requirements on the inclusive jet multiplicity:

Signal region(s)	SR0b		SR1b	SR3b
Jets req.	≥ 3 ($p_T > 50$ GeV)	≥ 5 ($p_T > 50$ GeV)	≥ 4 ($p_T > 50$ GeV)	–

As one can see, the SR0b selections were subdivided into two overlapping selections (≥ 3 or ≥ 5 jets, also denoted as SR0b5j and SR0b3j) to cover various signal scenarios that lead to differently jet-enriched final states. The optimal minimal number of jets and the jet p_T thresholds were defined as part of the DC14-based optimization, through a (m_{eff}, $E_{\text{T}}^{\text{miss}}$, #jets, jet p_T) scan similar to the one described below and focused on the few benchmark signal scenarios that were produced for DC14 studies. Only the p_{T} threshold for SR0b3j was raised from 40 to 50 GeV for homogenization among the SRs since this change had very small impact in the sensitivity.

All these selections are inclusive in terms of leptons ("at least two same-sign leptons"), it was found that for these early results no substantial gain would be achieved by considering trilepton final states separately (as was done in the Run-1 analysis) except for SR0b3j, where a $\geq$3 lepton requirement was found to improve

the sensitivity to slepton-mediated signals ($\tilde{g} \rightarrow q\bar{q}(\ell\ell/\ell\nu)\tilde{\chi}_1^0$).

To complete the definition of the signal regions, we added requirements on the effective mass m_{eff} and missing transverse momentum $E_{\text{T}}^{\text{miss}}$. We rely only on these two discriminant variables, well suited for generic SUSY searches, as one of the analysis strengths is to be sensitive to a broad range of BSM scenarios and we do not want to overtune it to a restricted set of benchmarks.

4.1 Optimization procedure and results

The optimization of the signal region definitions was carried on with the MC15 samples. We scanned the $(m_{\text{eff}}, E_{\text{T}}^{\text{miss}})$ plane for the four selections detailed above, looking at the impact of the cuts on various signal benchmarks. We used as figure of merit the signal discovery significance (Zn), calculated with `RooStats::NumberCountingUtils::BinominalObsZ` assuming an overall 40% systematic uncertainty on the background prediction (as a compromise to the 50% expected uncertainty on the fake-lepton background and 30% on the prompt-lepton background). We discarded the cut configurations where the background projection was too imprecise, due to limited MC statistics; more precisely when the statistical error on the projected background exceeded 30%. We also focused on signal benchmarks that would provide at least 2 signal events for the considered luminosity.

Figure 5 shows as an example the $(m_{\text{eff}}, E_{\text{T}}^{\text{miss}})$ planes for two different signal regions and models. The resulting maximum discovery significance across the signal grids and the corresponding $(m_{\text{eff}}, E_{\text{T}}^{\text{miss}})$ configurations are shown in Figure 6

for SR1b, SR3b and SR0b5j. As shown, with 2 fb^{-1} of data we can have sensitivity beyond the existing Run-1 limits in some of the models. Note that the Run-1 limits shown in the figures correspond to the best ATLAS limit, not necessarily obtained by the SS/3L analysis.

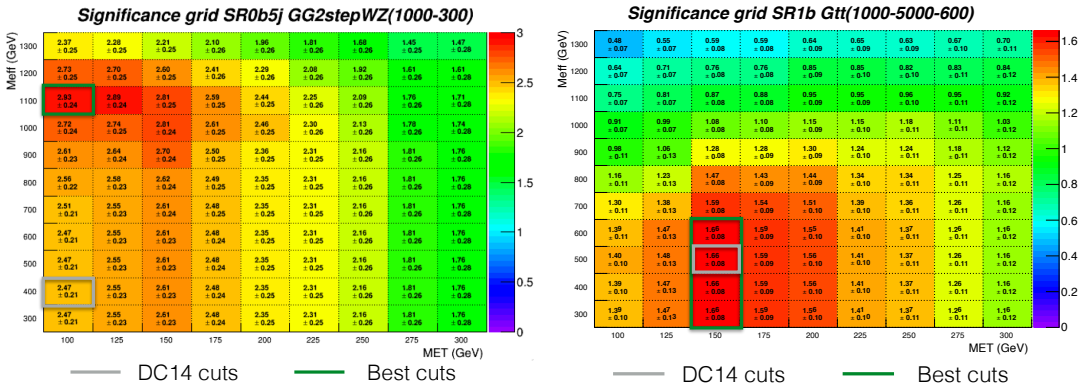

Figure 5: Example of ($E_{\mathrm{T}}^{\mathrm{miss}}$, m_{eff}) scans for SR0b5j (left) and SR3b (right). The configurations with maximum significance are highlighted as well as the outcome of the DC14 optimization studies.

4.2 Signal regions

The definition of the exact SR was done as a good compromise across the signal grids shown in Figure 6 with a single ($E_{\mathrm{T}}^{\mathrm{miss}}$, m_{eff}) configuration. Tables 2-4 show the optimized signal region definitions for scenarios with 2, 3 and 4 fb^{-1} respectively. The final SR to be used for the 2015 analysis was determined by the luminosity available at the end of the data-taking period: if less than 2.5 fb^{-1} had been available for analysis after GRL, we would have used the SRs for the 2 fb^{-1} scenario; if more than 3.5 fb^{-1} had been available, we would have used the SRs for the 4 fb^{-1} scenario. But with the 3.2 fb^{-1} eventually collected, we used the definitions corresponding to the intermediate scenario of 3 fb^{-1}. Figures 7

and 8 show the significance values obtained for those signal regions in the SUSY models considered, with the 1.64σ discovery contours extending beyond the Run-1 exclusions, even achieving a 3σ sensitivity in certain regions of the mass parameter space.

Table 2: Signal regions definition for the 2 fb^{-1} scenario (to be used for $L < 2.5$ fb^{-1}). The two leading leptons are required to have $p_{\mathrm{T}} > 20$ GeV .

Signal region	N_{lept}	$N^{20}_{b-\mathrm{jets}}$	N^{50}_{jets}	$E^{\mathrm{miss}}_{\mathrm{T}}$ [GeV]	m_{eff} [GeV]
SR3b	$\geq$2	$\geq$3	-	>100	>600
SR1b	$\geq$2	$\geq$1	$\geq$4	>125	>500
SR0b5j	$\geq$2	==0	$\geq$5	>100	>600
SR0b3j	$\geq$3	==0	$\geq$3	>150	>500

Table 3: Signal regions definition for the 3 fb^{-1} scenario (to be used for $2.5 \leq L < 3.5$ fb^{-1}), the one eventually used in this analysis. The two leading leptons are required to have $p_{\mathrm{T}} > 20$ GeV .

Signal region	N_{lept}	$N^{20}_{b-\mathrm{jets}}$	N^{50}_{jets}	$E^{\mathrm{miss}}_{\mathrm{T}}$ [GeV]	m_{eff} [GeV]
SR3b	$\geq$2	$\geq$3	-	>125	>650
SR1b	$\geq$2	$\geq$1	$\geq$4	>150	>550
SR0b5j	$\geq$2	==0	$\geq$5	>125	>650
SR0b3j	$\geq$3	==0	$\geq$3	>200	>550

Table 4: Signal regions definition for the 4 fb^{-1} scenario (to be used for $L \geq 3.5$ fb^{-1}). The two leading leptons are required to have $p_{\mathrm{T}} > 20$ GeV .

Signal region	N_{lept}	$N^{20}_{b-\mathrm{jets}}$	N^{50}_{jets}	$E^{\mathrm{miss}}_{\mathrm{T}}$ [GeV]	m_{eff} [GeV]
SR3b	$\geq$2	$\geq$3	-	>125	>700
SR1b	$\geq$2	$\geq$1	$\geq$4	>150	>600
SR0b5j	$\geq$2	==0	$\geq$5	>125	>700
SR0b3j	$\geq$3	==0	$\geq$3	>200	>600

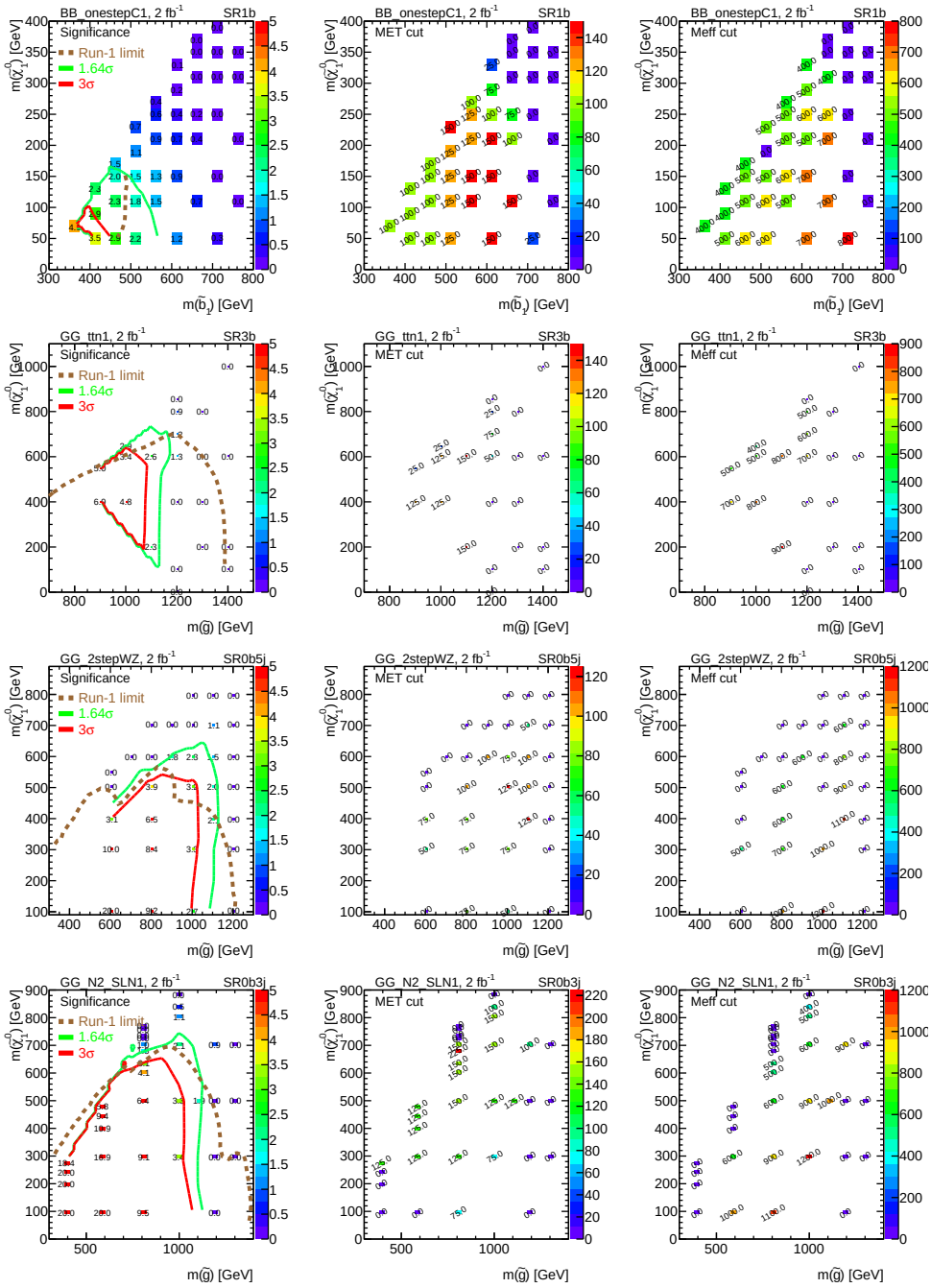

Figure 6: Maximum discovery significance (left) for 2 fb^{-1}, as well as the $E_{\mathrm{T}}^{\mathrm{miss}}$ (center) and m_{eff} (right) cuts needed to maximize the significance for: (from top to bottom) SR1b in the $\tilde{b}_1\tilde{b}_1^* \rightarrow t\bar{t}\tilde{\chi}_1^+\tilde{\chi}_1^-$ grid, SR3b in the $\tilde{g}\ \tilde{g}\ \rightarrow t\bar{t}t\bar{t}\tilde{\chi}_1^0\tilde{\chi}_1^0$ grid, SR0b5j in the $\tilde{g}\ \tilde{g}$ with $\tilde{g}\ \rightarrow q\bar{q}'WZ\tilde{\chi}_1^0$ grid and SR0b3j in the $\tilde{g}\ \tilde{g}$ with $\tilde{g}\ \rightarrow q\bar{q}(\ell\ell/\ell\nu)\tilde{\chi}_1^0$ grid. The Run-1 limits in those models are shown with a brown line, and the 1.64σ and 3σ discovery contours from the proposed signal regions are shown in green and red, respectively.

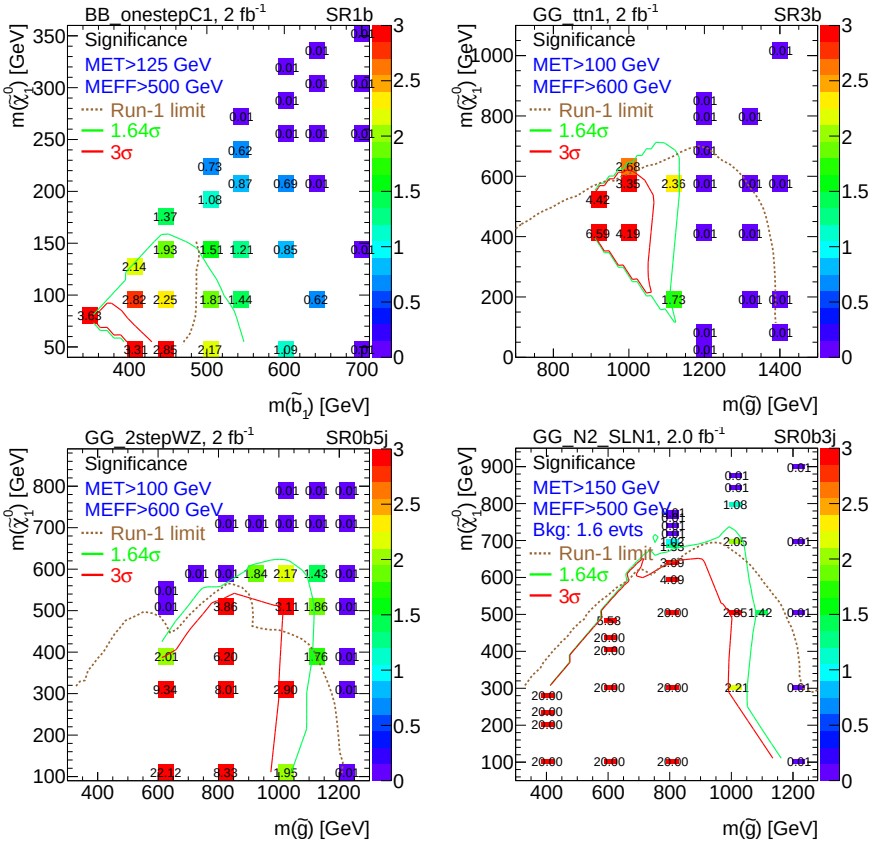

Figure 7: Discovery significance for the SRs defined in Table 2 (2 fb^{-1}) for SR1b in the $\tilde{b}_1\tilde{b}_1^* \to t\bar{t}\tilde{\chi}_1^+\tilde{\chi}_1^-$ grid (top left), SR3b in the $\tilde{g}\ \tilde{g}\ \to t\bar{t}t\bar{t}\tilde{\chi}_1^0\tilde{\chi}_1^0$ grid (top right), SR0b5j in the $\tilde{g}\ \tilde{g}$ with $\tilde{g}\ \to q\bar{q}'WZ\tilde{\chi}_1^0$ grid (bottom left) and SR0b3j in the $\tilde{g}\ \tilde{g}$ with $\tilde{g}\ \to q\bar{q}(\ell\ell/\ell\nu)\tilde{\chi}_1^0$ grid (bottom right). The Run-1 limits in those models are shown with a brown line, and the 1.64σ and 3σ discovery contours from the proposed signal regions are shown in green and red, respectively.

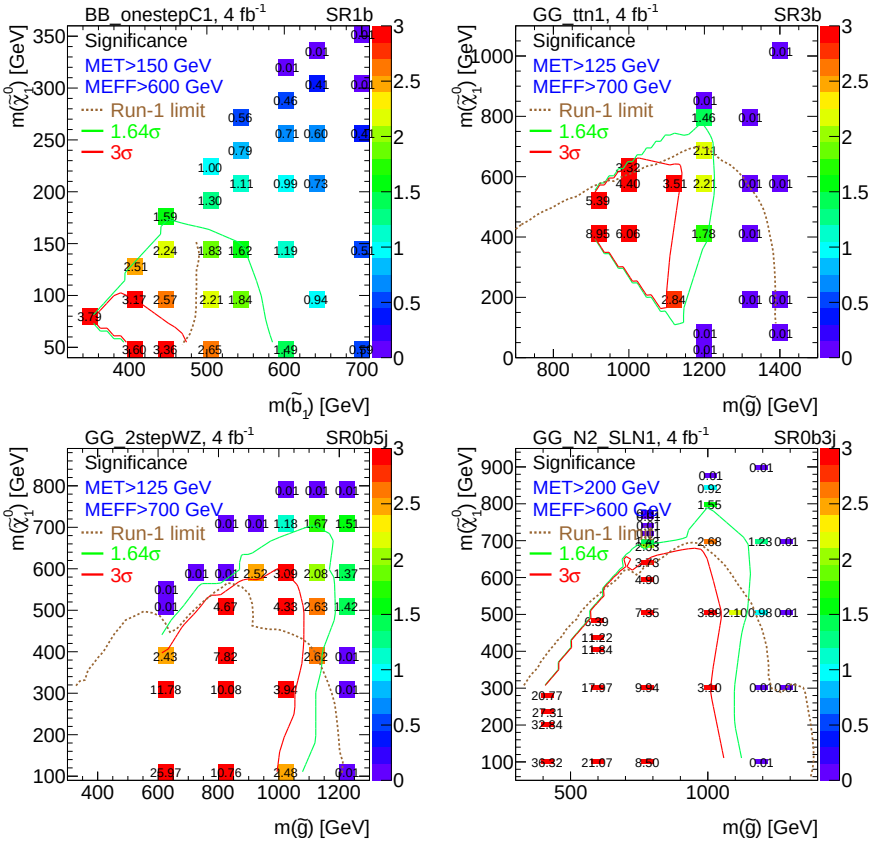

Figure 8: Discovery significance for the SRs defined in Table 4 (4 fb^{-1}) for SR1b in the $\tilde{b}_1\tilde{b}_1^* \to t\bar{t}\tilde{\chi}_1^+\tilde{\chi}_1^-$ grid (top left), SR3b in the $\tilde{g}\ \tilde{g}\ \to t\bar{t}t\bar{t}\tilde{\chi}_1^0\tilde{\chi}_1^0$ grid (top right), SR0b5j in the $\tilde{g}\ \tilde{g}$ with $\tilde{g}\ \to q\bar{q}'WZ\tilde{\chi}_1^0$ grid (bottom left) and SR0b3j in the $\tilde{g}\ \tilde{g}$ with $\tilde{g}\ \to q\bar{q}(\ell\ell/\ell\nu)\tilde{\chi}_1^0$ grid (bottom right). The Run-1 limits in those models are shown with a brown line, and the 1.64σ and 3σ discovery contours from the proposed signal regions are shown in green and red, respectively.